# Evaluating the role of sediment-bacteria interactions on *Escherichia coli* concentrations at beaches in southern Lake Michigan

Pramod Thupaki,[1] Mantha S. Phanikumar,[1] David J. Schwab,[2] Meredith B. Nevers,[3] and Richard L. Whitman[3]

[1] Association of bacteria with suspended sediment in the water column complicates the assessment and prediction of nearshore water quality. We examine the impact of sediment-bacteria interactions on *Escherichia coli* (EC) levels at beaches in southern Lake Michigan using three-dimensional EC fate and transport models with and without explicit descriptions of sediment-bacteria interactions. We simulate hydrodynamics using a nested-grid numerical model and use a semiparametric wave model to compute wave heights and net bottom shear stress. The attachment-detachment dynamics of bacteria in the water column are modeled using a linear partition coefficient. The numerical models were tested against data, collected in summer 2008, which included measurements of EC at three beaches and multiple ADCP deployments for currents and waves. Our results indicate that the model that accounts for sediment-bacteria interactions describes the observed data significantly better and that sediment, directly and indirectly, interacts with bacteria to influence their fate and transport. The improvement results from the model's ability to describe the multiple short-duration, low-intensity resuspension events at our sampling sites. A major resuspension event was noted during the simulation period but the sampling frequency during the event was inadequate to resolve the details of the peak. Using the linear isotherm model to simulate attachment-detachment dynamics of bacteria in the water column, we found that the fraction of bacteria attached to suspended sediment particles in the water column is highly variable in the vertical at offshore locations but nearly constant closer to the shore.

## 1. Introduction

[2] Suspended sediment particles in storm water runoff carry high levels of bacteria and viruses, which are eventually transported to downstream receiving water bodies posing significant human health risks at both marine and freshwater beaches. Earlier studies indicate that a majority of the fecal indicator bacteria (FIB) such as *Escherichia coli* (EC) are associated with fine particles smaller than about 60 μm [*Jeng et al.*, 2005; *Brown et al.*, 2013]. Association of bacteria with sediment particles [*Hipsey et al.*, 2006] complicates the mathematical description of fate and transport processes as bacteria associated with suspended particles tend to settle out of the water column and may experience favorable bed sediment conditions that prolong survival [*Sherer et al.*, 1992]. Resuspension of sediment-bound bacteria under favorable conditions can increase the levels of bacterial contamination in the water column. Water clarity controls light penetration and, therefore, the bacterial inactivation (loss per unit time) due to direct DNA damage caused by UV radiation. Hence, environmental conditions in the water column and bottom sediment layer influence key processes (such as settling) that determine the fate of indicator bacteria in the nearshore region (Figure 1).

[3] Settling of bacteria attached to suspended sediment represents a temporary removal mechanism from the water column. The sediment layer, with its high nutrient concentration, relative lack of predators, and little sunlight, provides a favorable environment for survival and potential growth of bacteria [e.g., *Davies et al.*, 1995; *Desmarais et al.*, 2002; *LaBelle et al.*, 1980; *Roper and Marshall*, 1979; *Sherer et al.*, 1992; *Savage*, 1905]. Creation of

[1]Department of Civil and Environmental Engineering, Michigan State University, East Lansing, Michigan, USA.

[2]Graham Environmental Sustainability Institute, U-M Water Center, University of Michigan, Ann Arbor, Michigan, USA.

[3]United States Geological Survey, Great Lakes Science Center, Porter, Indiana, USA.

Corresponding author: M. S. Phanikumar, Department of Civil and Environmental Engineering, Michigan State University, 1449 Engineering Research Court, Rm. A130, East Lansing, MI 48823, USA. (phani@msu.edu)
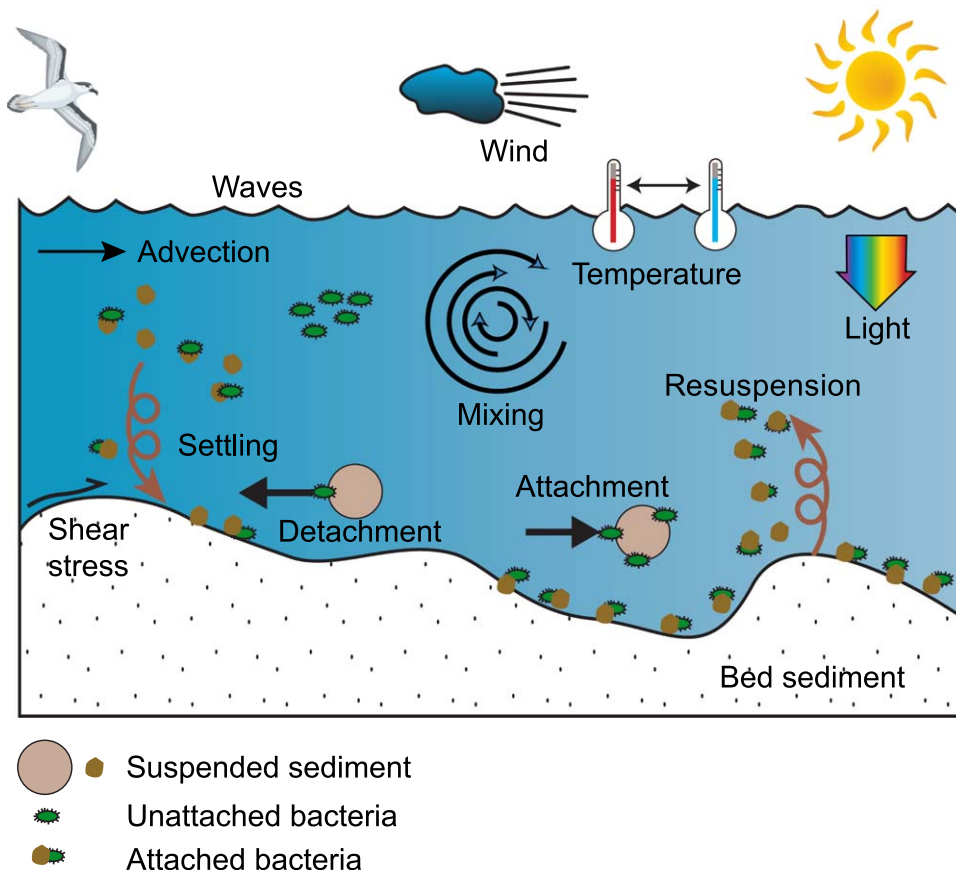
**Figure 1.** Conceptual diagram showing key processes modeled.

biofilms also enables bacterial communities to survive and potentially grow in the bottom sediment layer [*Decho*, 2000]. Survival and regrowth of bacteria in the bottom sediment have been observed to be significant in tropical watersheds [*Fujioka et al.*, 1998; *Hardina and Fujioka*, 1991], foreshore sand in surf zones [*Whitman and Nevers*, 2003], and marine wetlands [*Sanders et al.*, 2005]. Sediment resuspension due to high bottom shear stress introduces bacteria and sediment from the bottom sediment into the water column [*Eadie et al.*, 2002]. With the sediment layer acting as a reservoir for bacteria, sediment resuspension events can be a significant source of FIB at marine [*Phillips et al.*, 2011] and freshwater beaches [*Whitman and Nevers*, 2003; *Ge et al.*, 2010, 2012a, 2012b].

[4] The settling rate of unattached bacteria in the water column is generally negligible due to the small size of the bacterium (<1 μm diameter) [*Kirchman*, 1983]. However, attached bacteria settle at different rates depending on the characteristics of the substrate particle [*Auer and Niehaus*, 1993]. The fraction of attached bacteria is variable and depends on a number of environmental factors. There is evidence to suggest that EC tend to attach to suspended particles over a wide range of diameters and that although the association tends to change with the size of the storm event [*Brown et al.*, 2013; *Krometis et al.*, 2007], most studies found preferential attachment to finer particles in the range 0.45–30 μm [*Jeng et al.*, 2005]. Some studies [*Auer and Niehaus*, 1993; *Sinton*, 2005; *Hipsey et al.*, 2006] have reported that between 80 and 100% of the bacteria can be attached to sediment particles while *Jeng et al.* [2005] found that 85% of the EC in their study did not settle. Based on their data, *Jeng et al.* [2005] estimated an attached fraction (ratio of attached to unattached bacteria) of 0.22 for EC at a site near Lake Pontchartrain in Louisiana and a weighted-average settling velocity of 6.3 m/d for EC attached to particles in two size classes—fine (between 0.45 and 30 μm) and coarse (>30 μm). Numerical models simulating EC fate and transport in the past have used values of attached fraction ranging from 0.1 [*Liu et al.*, 2006; *Thupaki et al.*, 2010] to 1.0 [*Ge et al.*, 2012b; *de Brauwere et al.*, 2011].

[5] A number of environmental factors affect the attachment-detachment kinetics of bacteria to sediment particles. Studies by *Ginn et al.* [2002], *Guber et al.* [2005], *Li and McLandsborough* [1999], and *Lytle et al.* [1999] found that the Gram negative/positive nature of the bacterium, pH, ionic strength, salinity, and sediment characteristics are some of the factors that determine the attachment-detachment rates of bacteria to suspended sediment in the water column. *Lindqvist and Enfield* [1992] found that the relative concentrations of bacteria and suspended sediment strongly affect the attached fraction by increasing the number of available attachment sites. Therefore, as concentrations of suspended sediment in the water column decrease, the lack of available attachment sites reduces the fraction of attached bacteria. *Guber et al.* [2005] found that in the presence of organic material such as manure, the attached fraction of bacteria is nonlinearly related to the suspended sediment concentration.

[6] In addition to settling, bacteria undergo die-off due to predation, natural mortality, and direct DNA damage caused by factors such as sunlight and elevated temperatures [*Sinton et al.*, 2002; *King et al.*, 2008]. Using a detailed budget analysis based on the results of a three-dimensional numerical model, *Thupaki et al.* [2010] found that inactivation of bacteria due to sunlight is a major component of total bacterial loss in the water column at open beaches. Scattering and absorption of solar radiation in the water column depend on a number of factors. Algae, plankton, dissolved organic matter, suspended particulates, and organic detritus interact with specific wavelengths and their size and concentration determine the net extinction rate of light in the water column. Using data from a study that involved light-bag/dark-bag experiment and light-meters deployed at our beach sites (shown in Figure 2) in southern Lake Michigan, *Ge et al.* [2012b] estimated the base mortality rate of EC to be 0.0324/h and light-based inactivation rate to be $1.254 \times 10^{-4}$ m$^2$/(W h) for the summer 2008 conditions examined here.

[7] Suspended sediment concentrations within the water column are highly variable. Resuspension of bottom sediment due to current and wave action and input from rivers are major sources of suspended sediment in the coastal region. Southern Lake Michigan is a low-wave energy environment with a mean wave height of approximately 0.2 m during the summer 2008 period considered in this study. However, resuspension due to episodic events are more common in the shallow waters due to higher bottom stress. *Eadie et al.* [2002] have shown that episodic events associated with storms are responsible for sediment resuspension and nutrient cycling, and support algal communities in Lake Michigan. Using a two-dimensional sediment resuspension and transport model, *Lee et al.* [2005] found that the model results are highly sensitive to the sediment availability and settling rate and that southern Lake Michigan is a low-depositional environment. Field studies by *Eadie* [1997] using sediment traps have shown that the settling velocity is about 1 m/d in the nearshore region of Lake Michigan. This value is also comparable to the settling velocity values observed in Lake Pontchartrain by *Jeng et al.* [2005].

[8] A novel component of the present work is the application of fully three-dimensional hydrodynamic, wave, suspended sediment, and bacterial fate and transport models to Great Lakes beaches. The objectives of this study were to develop and test a coupled sediment resuspension and bacterial fate and transport model that simulates the interactions between bacteria and sediment (both suspended sediment within the water column and the bed sediment). Specifically, we seek to: (a) evaluate the role of sediment-bacteria interactions on bacterial concentrations in shallow and deep waters; (b) determine how the attached fraction of bacteria varies with time and depth; (c) determine how often sediment resuspension events occur in the nearshore region of Lake Michigan; and (d) using standard metrics such as the root mean squared error (RMSE), quantify gains in the model's ability to predict observed EC levels by explicitly including sediment-bacteria interactions. While a few studies have examined sediment-bacteria interactions using numerical models of varying complexity [e.g., *Gao et al.*, 2011, 2013; *Feng et al.*, 2013; *Chao*
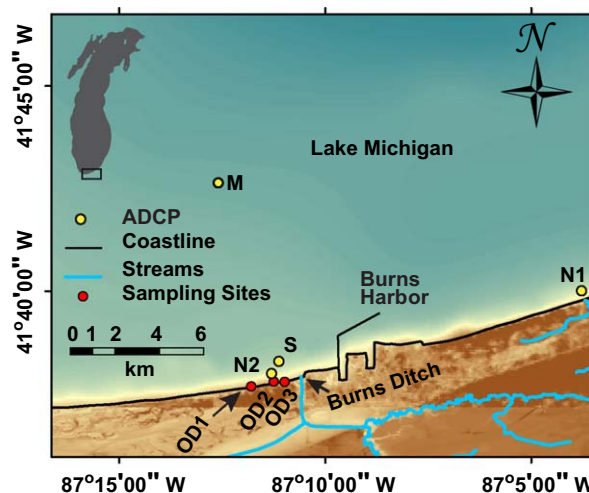


**Figure 2.** Map of Southern Lake Michigan showing the coastline (black solid line), major tributaries draining into the lake (blue solid lines) within the study area and locations of the ADCPs deployed during summer 2008 (yellow circles). Water samples were collected at three beaches in Ogden Dunes, Indiana (marked as OD1, OD2, and OD3). M, S, N1, N2 mark the locations where ADCPs were deployed to measure currents and waves.

*et al.*, 2008], we used an observational data set consisting of approximately twice-daily water samples as well as wave and hydrodynamic measurements in the nearshore region. The hydrodynamic, conservative tracer (Rhodamine WT), and thermal transport models were tested earlier and the results were reported in the work of *Thupaki et al.* [2013]. The GLERL-Donelan wave model used in our work was described in [*Schwab et al.*, 1984; *Liu et al.*, 1984] and has been extensively tested in the Great Lakes and was used to simulate surface waves. In addition, simultaneous light-bag and dark-bag experiments reported by *Ge et al.* [2012b] provided independent estimates of the natural mortality and light-based inactivation rates. These estimates are expected to better constrain the fate and transport models used in the present study with and without sediment processes.

## 2. Methods and Material

### 2.1. Study Site

[9] Hourly wave data were collected by four bottom-mounted, up-looking ADCPs deployed at locations M, S, N1, and N2 near the Burns Ditch outfall in southern Lake Michigan (Figure 2). Water samples were collected in knee-deep waters at the Ogden Dunes beaches (OD1, OD2, and OD3) that are part of the Indiana Dunes National Lakeshore as well as at the nearby outfall of Burns Ditch. Water samples were analyzed for *E. coli* concentrations using the Colilert-18 method [*American Public Health Association (APHA)*, 1998]. Turbidity was measured at the Ogden Dunes beach sites and at the Burns Ditch site using a YSI sonde (model 6600) and later converted to suspended sediment concentration using a relation between the two variables at the sites. During the same period, light-bag and dark-bag experiments were conducted to estimate the base

mortality, light extinction coefficients, and light-based inactivation rates. The details of these experiments are described by *Ge et al.* [2012b]. For offshore locations, the magnitude of acoustic backscatter recorded by ADCPs can be used to calculate the concentration of suspended sediment in the water column [*Wall et al.*, 2006]. The suspended sediment concentration at location S was calculated using a relation between SSC and backscatter intensity as described by *Lee et al.* [2005].

## 2.2. Hydrodynamic and Wave Models

[10] Lake-wide circulation was simulated using a hydrodynamic (current) model based on the Princeton Ocean Model [*Blumberg and Mellor*, 1987]. For computational efficiency and accuracy, a lake-wide grid with coarse resolution (2 km) was coupled to a high-resolution nearshore model with 100 m grid resolution. The coupling between the lake-wide and nearshore models was one-way and offline and implemented by interpolating results from the coarse-grid model to provide boundary conditions for the nearshore model.

[11] Wave heights were simulated using the GLERL-Donelan wave model described by *Schwab et al.* [1984]. Details of this model are provided in Appendix A. Comparisons with observations as well as with results from other wave models by *Schwab et al.* [1984] and *Liu et al.*, 1984, 2002] have shown that the model predicts wave heights in Lake Michigan accurately. The results from the wave and current models were used to calculate net bottom shear stress and to couple the three-dimensional sediment transport model with the bacterial fate and transport model as described in the following sections.

## 2.3. Suspended Sediment Transport Model

[12] Suspended sediment concentration in the water column was modeled using a three-dimensional advection dispersion equation (1):

$$\frac{\partial S}{\partial t} + u\frac{\partial S}{\partial x} + v\frac{\partial S}{\partial y} + w\frac{\partial S}{\partial z} = \frac{\partial}{\partial x}\left(K_H \frac{\partial S}{\partial x}\right) + \frac{\partial}{\partial y}\left(K_H \frac{\partial S}{\partial y}\right) + \frac{\partial}{\partial z}\left(K_V \frac{\partial S}{\partial z}\right) - \frac{\partial F_{SS}}{\partial z} \quad (1)$$

$$F_{SS} = w_S S \quad (2)$$

where $S$ is the suspended sediment concentration (SSC) in kg/m$^3$, $w_S$ is the settling velocity of suspended sediment particles, and $F_{SS}$ is the settling "loss" term expressed as a flux.

[13] Bottom boundary condition for solving the suspended sediment transport model is shown in equation (3). The deposition and erosion (resuspension) fluxes $F_{SS}$ and $F_{RS}$ in equations (4) and (5) (units: kg/m$^2$ s) are based on the descriptions in the work of *Krone* [1962] and *Mehta and Partheniades* [1975] for cohesive sediments.

$$w_S S + K_V \frac{\partial S}{\partial z} = F_{SS} - F_{RS} \quad (3)$$

$$F_{SS} = \max\left[0, w_S S\left(1 - \frac{\tau_{bot}}{\tau_{cr,d}}\right)\right] \quad (4)$$

$$F_{RS} = \max\left[0, M\left(\frac{\tau_{bot}}{\tau_{cr,ero}} - 1\right)\right] \quad (5)$$

[15] Here $\tau_{bot}$ is the net bottom shear stress, $\tau_{cr,ero}$ is the critical shear stress for erosion, $\tau_{cr,d}$ is the critical shear stress for deposition, and $M$ is the erodibility coefficient in kg/m$^2$ s [*Rijn*, 1989]. A zero-flux boundary condition was used at the free water surface to close the system of equations as shown below:

$$w_S S + K_V \frac{\partial S}{\partial z} = 0 \quad (6)$$

## 2.4. Bacterial Fate and Transport Models

[16] The fate and transport of bacteria are simulated in this study using two different models. While both of them simulate three-dimensional advection and diffusion processes, the first (simpler) model uses a constant attached-fraction (to describe settling losses for bacteria) and solar extinction coefficient (to describe inactivation due to solar radiation). The second model explicitly describes sediment-bacteria interactions and dynamically calculates the attached-fraction and sunlight extinction rate in the three-dimensional computational domain using results from a coupled sediment transport model. These models are described below in greater detail.

### 2.4.1. Model I (Without Sediment-Bacteria Interactions)

[17] This model, similar to the one described in *Thupaki et al.* [2010] and shown in equation (7), includes advection and diffusion terms in three dimensions, natural mortality and inactivation of bacteria due to sunlight, and settling of a constant-in-time, "known" fraction of attached bacteria ($f_p$). A temperature correction factor that increases the overall loss rate as temperature increases is also included.

$$\frac{\partial C}{\partial t} + u\frac{\partial C}{\partial x} + v\frac{\partial C}{\partial y} + w\frac{\partial C}{\partial z} = \frac{\partial}{\partial x}\left(K_H \frac{\partial C}{\partial x}\right) + \frac{\partial}{\partial y}\left(K_H \frac{\partial C}{\partial y}\right) + \frac{\partial}{\partial z}\left(K_v \frac{\partial C}{\partial z}\right) - f_p \frac{\partial w_S}{\partial z} C - k_{net} C \quad (7)$$

$$k_{net} = \left(k_I I_0(t)e^{-k_e z} + k_d\right)\alpha^{T-20} \quad (8)$$

where $C$ denotes the EC concentration (CFU/100 mL) and $x$, $y$, $z$, $t$ denote the three space coordinates and time. The net loss rate for bacteria in the water column ($k_{net}$) includes contributions from the inactivation due to sunlight ($k_I$) which depends on the solar radiation ($I_0$) and the light extinction coefficient ($k_e$), the base mortality rate ($k_d$), and $\alpha$, a temperature correction factor for the overall loss rate. Settling loss of bacteria attached to suspended sediment is determined based on a constant ($f_p$) and settling velocity ($w_s$). The horizontal mixing coefficient ($K_H$) was calculated using the Smagorinsky turbulence closure model [*Smagorinsky*, 1963] while the vertical mixing coefficient ($K_V$) was calculated using the Mellor-Yamada turbulence closure model [*Mellor and Yamada*, 1982]. Additional details about the turbulence closure models used and the three-dimensional transport equation are available in any standard text on numerical ocean modeling [e.g., *Vallis*, 2006].

### 2.4.2. Model II (With Sediment-Bacteria Interactions)

[18] In this section, we present a three-dimensional sediment-bacteria interactions model to simulate EC and

sediment concentrations in the water column and the bottom sediment layer. The physical and biological processes included in the model are first described followed by mathematical descriptions of the model. When sediment-bacteria interactions are directly modeled, the attached fraction can be calculated from the model instead of treating it as an input parameter. Separate equations can be written for the attached and unattached bacteria as described in the work of *Gao et al.* [2013, 2011] who used a two-dimensional, vertically integrated form of the equations and solved for the total concentration of bacteria. The unattached bacteria are assumed not to settle; however, the attached bacteria can undergo settling and resuspension.

[19] There are different ways to describe the interactions between bacteria and sediment. Available work in this area appears to make use of the assumption of "fast" attachment-detachment kinetics [*Gao et al.*, 2013, 2011; *Bai and Lung*, 2005] leading to a local equilibrium characterized by an equilibrium or partition coefficient ($K_D$). The attachment-detachment processes are assumed to be fast relative to the time scales associated with other processes such as advection and dispersion. The basis for this assumption appears to come from a number of groundwater investigations [e.g., *Reddy and Ford*, 1996; *Scholl and Harvey*, 1992; *Lindqvist and Enfield*, 1992] as well as the work of *Chapra* [2008]. We note that it is also possible to make exactly the opposite assumption, i.e., "slow" or irreversible attachment-detachment kinetics based on some available evidence that bacteria, once attached, remain attached by bridging of extracellular polymers [*Jamieson et al.*, 2005; *Abu-Ashour*, 1994]. Models based on these assumptions can be expected to produce very different results.

[20] If the "fast" kinetics assumption is invoked, then all that is needed is a linear partition coefficient ($K_D$) to describe interactions between bacteria and sediment particles. This formulation has the advantage of being able to specify the ratio of unattached to attached bacteria without explicitly modeling the attachment and detachment kinetics as shown below and by *Gao et al.* [2011]. On the other hand, if the assumption of slow or irreversible attachment-detachment kinetics is used, then the unattached and attached bacterial populations do not interact. An evaluation of the two approaches is not the focus of the present study. We have used the first approach based on previous experience from modeling heavy metal transport where solving a single equation for the total concentration is preferred [*Wu et al.*, 2005; *Gao et al.*, 2011].

[21] Assuming that the time scale for attachment-detachment kinetics is much faster than advection and diffusion, we obtain the following equation for the total concentration of bacteria in the water column by adding two separate equations for the attached and unattached bacteria [*Gao et al.*, 2013]:

$$\frac{\partial C_T}{\partial t} + u\frac{\partial C_T}{\partial x} + v\frac{\partial C_T}{\partial y} + w\frac{\partial C_T}{\partial z} = \frac{\partial}{\partial x}\left(K_H\frac{\partial C_T}{\partial x}\right)$$
$$+ \frac{\partial}{\partial y}\left(K_H\frac{\partial C_T}{\partial y}\right) + \frac{\partial}{\partial z}\left(K_v\frac{\partial C_T}{\partial z}\right) - k_{net}C_T - \frac{\partial F_{SC}}{\partial z} \quad (9)$$

$$k_{net} = \left(k_I I_0(t)e^{-k_e z} + k_d\right)\alpha^{T-20} \quad (10)$$

$$F_{SC} = w_S C_P \quad (11)$$

[22] Here $C_T$ is the total EC concentration in CFU/m$^3$ (total concentration of bacteria ($C_T$) = concentration of unattached bacteria ($C_D$) + concentration of attached bacteria ($C_P$). Settling flux of bacteria attached to suspended sediment in the water column is included in equation (9), using the term $F_{SC}$. Here $w_S$ is the settling velocity and $C_P$ is the volume-specific concentration of attached EC (CFU/m$^3$). Due to the highly turbulent nature of flow in the nearshore and the extremely small size of the individual bacteria, settling flux of unattached bacteria in the water column is assumed to be negligible [*Hipsey et al.*, 2008]. The Stokes velocity is often used to compute the terminal settling velocity of sediment particles in quiescent water as a function of particle size and density. *Characklis et al.* [2005] and *Soupir et al.* [2008] have shown that EC display preferential attachment to sediment particles between 3 and 63 μm. Therefore, a single sediment class is modeled. When they settle, however, sediment particles do not settle individually but in flocs, which are formed due to particle collisions and surface electrochemical charges. A variable flock diameter that depends on these factors is often used for settling velocity in cohesive sediment transport models [*Chao et al.*, 2008; *Lee et al.*, 2005]. Therefore, in general, settling velocity will not be a single number in the model but varies over time and space. There are a number of factors that influence the formation and breakup of flocs. One of the major factors is the suspended sediment concentration itself. Other factors include fluid shear stress and temperature. Based on available evidence in the literature, the dependence of settling velocity on local suspended sediment concentration follows three regimes [*Mehta*, 1983]: (1) free settling described by Stoke's law for SSC values below 300 mg/L, (2) flocculation settling for SSC values above 300 mg/L and below 10,000 mg/L, and (3) hindered settling for SSC values above this limit. The maximum observed concentrations at our beach sites are below 20 mg/L, therefore flocculation effects are expected to be minimal at the beach sites although they may be important closer to the source. We used a single constant value of settling velocity for such low concentrations as was done by others in the past [*Lumborg*, 2005]. The settling velocity is an important input to the model. The single settling value used in equation (11) typically represents the weighted-average settling velocity over the different size classes with which bacteria are associated. A LISST-100X instrument was deployed at the site to obtain information on particle size distribution; however, the instrument malfunctioned and did not record any useful data. In the absence of this information, the settling velocity value used is based on earlier field studies in Lake Michigan and other lakes. Observations by *Eadie* [1997] at Lake Michigan sites gave estimates of about 1 m/d for settling velocity within the epilimnion. *Jeng et al.* [2005] estimated a weighted-average settling velocity of 0.272 m/h for *E. coli* (i.e., 6.53 m/d) at a site in Lake Pontchartrain in Louisiana. After examining the sensitivity of this parameter on model results, we chose a value of 5 m/d in this study, which roughly corresponds to the settling velocity calculated using Stoke's law for a fine silt particle of diameter 10 μm [*Jeng et al.*, 2005] with a density of 2650 kg/m$^3$. The same

value is used in both models to allow a direct comparison of results. We note that the median grain sizes found on bed sediments at many beach and river sites are significantly larger compared to the size of particles with which bacteria are associated. It is well known, however, that a direct calculation of settling velocity using Stoke's law and the median grain size can significantly overestimate the settling velocity due to a number of factors [*Rehmann and Soupir*, 2009; *Droppo et al.*, 2009; *Burban et al.*, 1990].

[23] Following *Chapra* [2008] and assuming that bacteria attach to sediment particles following a linear partition coefficient ($K_D$), we calculated the attached and unattached fractions of the bacteria using equations (12)–(18):

$$K_D = \frac{\zeta}{C_D} \tag{12}$$

$$f_P = \frac{K_D S}{1 + K_D S} \tag{13}$$

$$f_D = \frac{1}{1 + K_D S} \tag{14}$$

$$C_P = f_P C_T \tag{15}$$

$$C_D = f_D C_T \tag{16}$$

$$f_P + f_D = 1 \tag{17}$$

$$C_T = C_D + K_D S C_D \tag{18}$$

[24] Here $f_P$ and $f_D$ are the fractions of EC in the attached and unattached states, respectively. The value of the partition coefficient ($K_D$) has been determined to be around 0.1–0.001 L/g for saturated groundwater flow [*Gantzer et al.*, 2001; *Lindqvist and Enfield*, 1992; *Reddy and Ford*, 1996]. However, values of 0.01–10 L/g have been used by models to describe the attached fraction in freshwater systems [*Bai and Lung*, 2005; *Gao et al.*, 2011]. $\zeta$ is the mass-specific concentration of EC attached to suspended sediment in the water column, with units of CFU/kg [*Chapra*, 2008]. Suspended sediment increases light scattering and contributes to extinction of light in the water column. Using the computed three-dimensional value for suspended sediment concentration ($S$) at each time step, the extinction coefficient ($k_e$) in equation (10) was calculated using the following approximate relation: $k_e = 0.55 * S$ [*Chapra*, 2008].

### 2.4.3. Boundary Conditions

[25] Boundary conditions are needed to solve the three-dimensional equation (9) for the total EC concentration in the water column. If we consider a cell at the bottom, the sum of the advective (i.e., settling) and diffusive fluxes should be balanced by the difference between the erosional and depositional fluxes. Equations (19) and (20) show the resuspension and settling fluxes for EC at the interface between sediment layer and water column. The concentration of bacteria attached to sediment ($C_P$) is calculated using the same attachment-detachment kinetics described in equation (15). We close the systems of equations by

applying a zero-flux boundary condition at the water surface. Thus, we have for the bottom boundary condition:

$$w_S C_P + K_V \frac{\partial C_T}{\partial z} = F_{SC} - F_{RC} \tag{19}$$

$$F_{SC} = \max \left[ 0, w_S C_P \left( 1 - \frac{\tau_{bot}}{\tau_{cr,d}} \right) \right] \tag{20}$$

$$F_{RC} = F_{RS} C_{Sed}$$

[26] Here $F_{SC}$ and $F_{RC}$ are the settling and resuspension fluxes for attached bacteria and $C_{sed}$ is the mass-specific concentration of EC in the bed sediment. Equation (19) is based on the assumption that only the attached bacteria settle out of the water column (the first term on the left-hand side) but the total EC (i.e., both attached and unattached EC) are involved during exchange with the sediment bed. For an alternative form of this boundary condition, we can assume that only attached bacteria are strictly allowed in any type of exchange with the sediment bed:

$$w_S C_P + K_V \frac{\partial C_P}{\partial z} = F_{SC} - F_{RC}$$
$$\Rightarrow f_P w_S C_T + f_P K_V \frac{\partial C_T}{\partial z} = F_{SC} - F_{RC} \tag{21}$$

[27] The two boundary condition equations (19) and (21) differ by the fraction of attached bacteria multiplying the diffusive term on the left-hand side of the equations. We have used equation (19) in this paper. At the free surface at the top, we specify a zero-flux boundary condition as shown below:

$$w_S C_P + K_V \frac{\partial C_T}{\partial z} = 0 \tag{22}$$

### 2.4.4. Bottom Sediment Layer

[28] In a low-depositional environment such as the near-shore region of southern Lake Michigan, sediment availability determines resuspension fluxes during periods with large bottom shear stress. Earlier field studies in Lake Michigan [*Lee et al.*, 2005; our unpublished results] showed that fine sediment is limited to the top 5 mm of the bottom layer. The mass of sediment in the bottom sediment layer is calculated using equation (23). Here $m_{sed}$ is the mass of bed sediment per unit area in kg/m², $F_{SS}$ is the sediment settling (depositional) flux at the sediment-water interface, and $F_{RS}$ is the sediment resuspension flux (equations (4) and (5)).

$$\frac{\partial m_{sed}}{\partial t} = [F_{SS} - F_{RS}] \tag{23}$$

[29] As additional sediment mass is deposited on the lake bottom, sediment compaction occurs due to the weight of the sediment and the water column above. However, considering the relatively short time scales of interest, this study did not consider the dynamics of sediment compaction and burial. Equation (24) describes the concentration of bacteria in the bed sediment:

$$\frac{\partial C_{sed}}{\partial t} = \frac{F_{SS}}{m_{sed}}(\zeta - C_{sed}) - k_{net,sed}C_{sed} \tag{24}$$

[30] Here $C_{sed}$ is the concentration of bacteria in the sediment in CFU/kg. EC in the attached state ($C_P$) undergo settling and can survive/grow in the sediment layer. The growth dynamics of bacteria in the bottom sediment layer could be included in the overall growth/inactivation rate ($k_{net,sed}$) in equation (24). However, due to the lack of reliable data on the growth dynamics of EC in the bottom sediment layer, we assumed zero growth and zero inactivation rate ($k_{net,sed} = 0$) in the bottom sediment layer.

## 2.4.5. Bottom Shear Stress

[31] The net bottom shear stress is due to the combined action of currents and waves (equation (25)). Shear stress due to current ($\tau_c$) was calculated using equation (26) and following the example of *Luettich et al.* [1990] the bottom shear stress due to waves ($\tau_w$) was calculated using equation (27):

$$\tau_{bot} = \left(\tau_c^2 + \tau_w^2\right)^{1/2} \tag{25}$$

$$\tau_c = \frac{1}{2}\rho C_b\left(u^2 + v^2\right) \tag{26}$$

$$\tau_w = \frac{1}{2}\rho f_w U_b^2 \tag{27}$$

[32] Here $C_b$ is the bottom friction coefficient for currents, $f_w$ is the bottom friction coefficient for waves, and $U_b$, $A_b$ are the maximum wave orbital velocity and amplitude, respectively [*Chao et al.*, 2008]:

$$C_b = \left(\frac{\kappa}{\ln(\Delta z/2z_0)}\right)^2 \tag{28}$$

$$f_w = 2\left(\frac{U_b A_b}{v}\right)^{-1/2} \tag{29}$$

$$U_b = \frac{\pi H}{T\sinh(2\pi d/L)}$$
$$A_b = \frac{1}{2\sinh(2\pi d/L)} \tag{30}$$

[33] Assuming a logarithmic bottom boundary layer, the bottom friction coefficient ($C_b$) can be calculated using equation (28). Here $\kappa$ is the von Karman constant and the roughness height, $z_0$ was set to 0.8 mm or approximately 4 times the mean size of sand particles [*Lee et al.*, 2007] and $\Delta z/2$ is the height from the lake bottom where horizontal velocities ($u$, $v$) are evaluated as per the Arakawa C grid used in the Princeton Ocean Model. The wave friction factor $f_w$ has been calculated using equation (29) and the maximum orbital velocity $U_b$ and the maximum orbital amplitude ($A_b$), are given by equation (30). Here $d$ is the water depth and $L$ is the wavelength. Since sediment morphology was not the focus of the study, bottom shear stress calculations from the results of the wave model were coupled to the current model in an offline manner and impact of changes to the bathymetry over time (due to sediment deposition and erosion) on the hydrodynamic model are not considered.

**Table 1.** RMSE Values for Wave and Current Comparisons at Different Locations in the Nearshore Region

| Location ID (GPS) | Depth (m) | RMSE (m) (waves, $H_S$) | RMSE (m/s) (currents) |
|---|---|---|---|
| M (41.71059 N, 87.20996 W) | 18.3 | 0.113 | 0.031 |
| S (41.63813 N, 87.18539 W) | 9.6 | 0.123 | 0.037 |
| N1 (41.66677 N, 87.06297 W) | 4.1 | 0.127 | 0.048 |
| N2 (41.63315 N, 87.18839 W) | 5.2 | 0.147 | 0.042 |

## 3. Results

[34] Lake-wide circulation was resolved using a uniform grid with 2 km resolution and 20 vertical levels over the water column depth. Small-scale features in circulation close to the shoreline were resolved using a nested-grid model with 100 m resolution in the horizontal and 20 depth levels in the vertical. The lake-wide model was forced by wind stress and surface heat flux, while the nested-grid model included forcing at the open boundary based on results interpolated from the large-scale model. The hydrodynamic model was tested against currents measured by bottom-mounted ADCPs, located in the coastal boundary layer. Detailed analysis of the model results are presented in the work of *Thupaki et al.* [2013]. Table 1 provides a summary of the RMSE values for the hydrodynamic model comparisons.

[35] Results from the wave model are presented in Figures 3a and 3b, which show comparisons between the observed and simulated values of significant wave height ($H_S$) at location M (offshore) and location S (nearshore). Figures 3c and 3d show results of the wave model with observations made at depths of 5 m where the deep water linear wave theory is less applicable and shallow water effects such as refraction, diffraction, and wave breaking become more important. RMSE values for the numerical model at different locations in the offshore and nearshore locations in Table 1 show that error in the simulated wave height increases closer to the shoreline. However, peak wave heights on Julian Day (JD) 182 and JD 185 have been accurately predicted by the wave model. An examination of the observed wave power and direction spectra during the peak wave height events that occurred during the sampling period (not shown) indicated that waves during the resuspension events were from a NNW and NNE direction—directions in which the fetch length is maximum.

[36] Figure 4 shows a comparison between observed and simulated values of SSC at a location S (nearshore). The parameters used by the sediment resuspension model to simulate SSC in the water column are given in Table 2a. Since actual measurements of sediment thicknesses at different spatial locations were not available, the sediment model was initialized with uniform sediment mass. A parameter estimation exercise was conducted to identify values that provided optimal results. Using a uniform initial sediment distribution, a model spin-up period of several days was required.

[37] The Fourier norm calculated using equation (31) is a measure of the variance in the observed time series that is not predicted by the modeled time series. The normalized
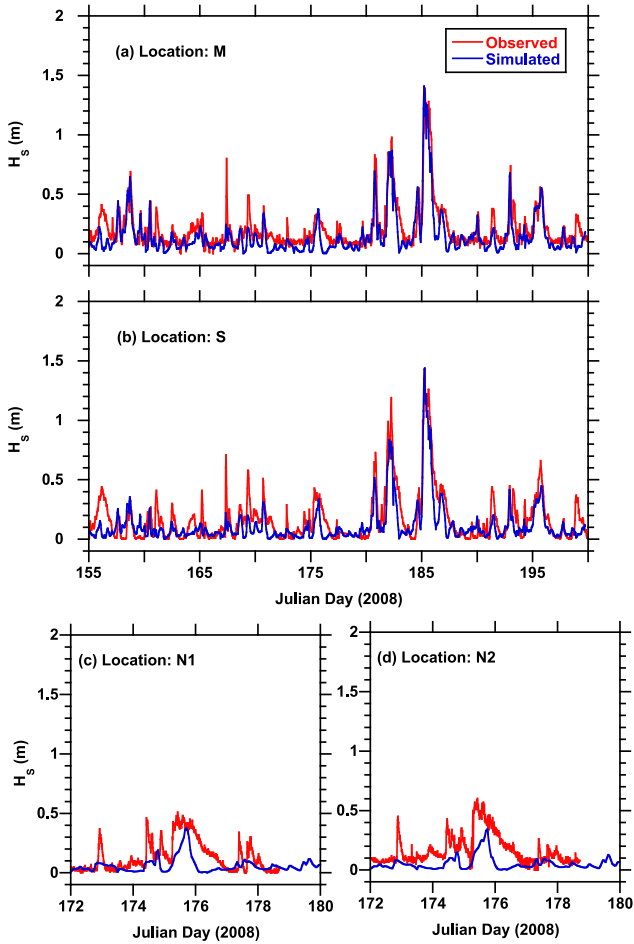
**Figure 3.** Significant wave height compared with ADCP observations at: (a) offshore location M and (b–d) near-shore location S, N1, and N2, respectively.

Fourier norms $(F_n = \|V_o, V_c\|/\|V_o, 0\|)$ have been calculated for 2 twenty-day intervals in the simulation period and are shown in Table 3. A value of $F_n = 0$ indicates a perfect match between observed $(V_o)$ and simulated $(V_c)$ time series and a value of $F_n < 1$ means that it is better than no prediction (or 0 wave height):

$$\|V_o, V_c\| = \left( \frac{1}{N} \sum_{t=1}^{N} |V_o, V_c|^2 \right)^{\frac{1}{2}} \tag{31}$$
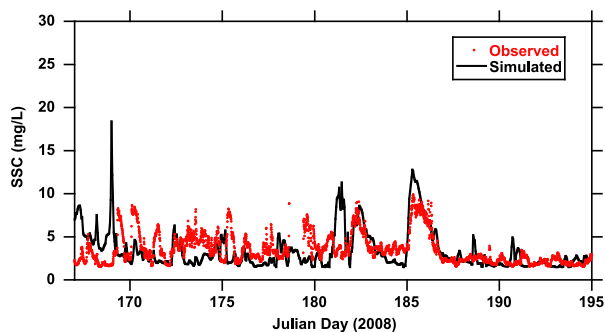


**Figure 4.** Observed and simulated values of suspended sediment concentration at location S.

**Table 2a.** Values of the Parameters Used in the Sediment and EC Fate and Transport Models

| Parameters | Value |
|---|---|
| Initial bottom sediment layer mass | 1.5 kg/m$^2$ |
| Critical shear stress for sediment deposition | 2.5 N/m$^2$ |
| Critical shear stress for sediment resuspension | 0.1 N/m$^2$ |
| Sediment settling rate | 5 m/d |
| Sediment erodability rate | $1 \times 10^{-6}$ kg/m$^2$ s |

**Table 2b.** Values of the Parameters Used in the EC Fate and Transport Model

| Parameters | Value |
|---|---|
| Base mortality rate for bacteria | $0.9 \times 10^{-5}$/s |
| Solar inactivation rate of bacteria | $3.48 \times 10^{-8}$/s |
| Temperature dependence of bacteria mortality ($\alpha$) | 1.07 |
| Initial *E. coli* concentration in bottom sediment layer | $5 \times 10^6$ CFU/kg |

[38] Figure 5 shows the comparison between observations at the Ogden Dunes beaches and results from the EC model with and without sediment-bacteria interactions for a 1 month simulation period corresponding to summer 2008 conditions. Parameters used in the models are presented in Table 2b. Since both models used the same set of formulations/parameters to describe hydrodynamics, horizontal and vertical mixing processes (e.g., dispersion coefficients), and the fate of bacteria in the water column (e.g., base mortality and light-based inactivation rates estimated from the light-bag and dark-bag experiments), differences in model results are only due to the presence or absence of sediment-bacteria interactions in the two models. Effect of uncertainties associated with culture-based microbiological methods and difficulties in sampling at the mouth of the outfall were simulated by perturbing the EC levels entering the computational domain from the Burns Ditch outfall by ±50%. The uncertainty bands for EC concentrations at the beaches are shown using cyan-colored error bars around the base case simulation (red solid line) in Figure 5. The base case simulation used an EC partition coefficient of 10 L/g, which corresponds to the value used by *Bai and Lung* [2005]. Several interesting observations can be made based on the comparisons in Figure 5. First, we note that the major peaks are captured by both models although the model without sediment processes significantly underpredicts the background concentrations and fails to capture the numerous smaller peaks due to resuspension events. The effect of sediment resuspension events during our simulation period was mainly to elevate the background levels of EC by producing several smaller peaks instead of a few isolated large peaks. There are several reasons for this

**Table 3.** Comparison of the Accuracy of the Wave Model in the Nearshore and Offshore Regions Expressed as a Normalized Fourier Norm

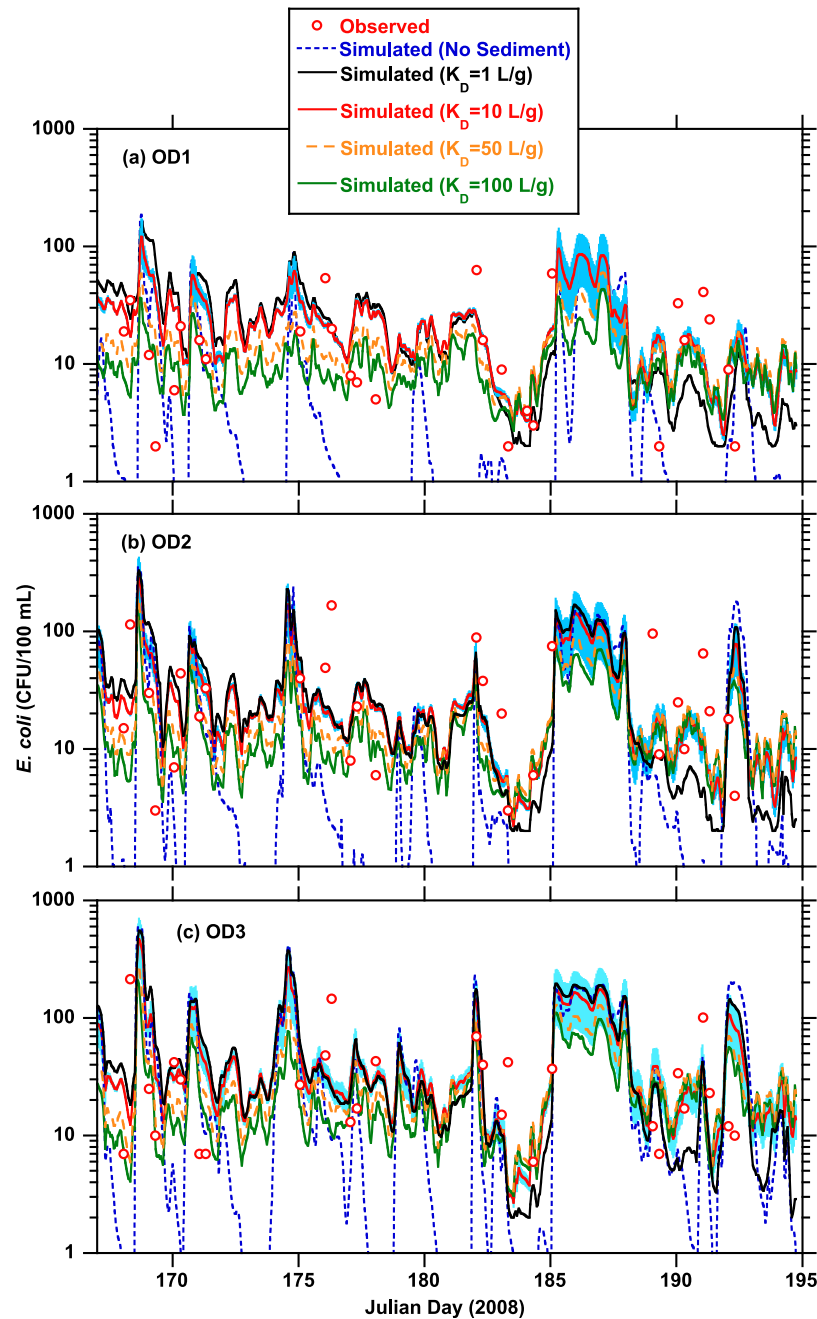| Location | $F_n$ (JD 160-JD 180) | $F_n$ (JD 180-JD 200) |
|---|---|---|
| S | 0.6436 | 0.3781 |
| M | 0.5649 | 0.3177 |

**Figure 5.** Observed (symbols) and simulated (lines) concentrations of *Escherichia coli* at: (a) Ogden Dunes beach OD1, (b) Ogden Dunes beach OD2, and (c) Ogden Dunes beach OD3; results from model with sediment-bacteria interaction (black, red, yellow, and green lines) and without sediment-bacteria interaction (blue dashed line). The red solid line represents the base case simulation (with a partition coefficient of 10 L/g) while the cyan-colored bands around the base case represent ± 50% uncertainty associated with input from the outfall.

result. All beach sites (OD1, OD2, and OD3) are impacted by contamination originating from the Burns Ditch outfall and the major peaks observed at the beach sites correspond to elevated levels of EC coming from the outfall with a time lag corresponding to the travel time between the outfall and the beach site. The model without sediment processes did not have any difficulty capturing these peaks as basic hydrodynamic and transport processes as well as light and dark mortality rates are already included in the model.

[39] To compare the performance of the two models (i.e., with and without sediment-bacteria interactions), we calculated the RMSE between EC values observed during the field study and values predicted by the model at the Ogden Dunes beaches using equation (32). RMSE values are summarized in Table 4:

**Table 4.** RMSE Values Between Observed and Modeled EC Values at the Ogden Dunes Beaches

| Case | Site | RMSE Value | | |
|---|---|---|---|---|
| | | No Sediment | With Sediment | % Improvement |
| $K_D = 1$ L/g | OD1 | 1.36 | 0.61 | 55.1 |
| | OD2 | 1.36 | 0.64 | 52.9 |
| | OD3 | 1.05 | 0.61 | 41.9 |
| $K_D = 10$ L/g | OD1 | 1.36 | 0.52 | 61.7 |
| | OD2 | 1.36 | 0.53 | 61.0 |
| | OD3 | 1.05 | 0.56 | 46.7 |
| $K_D = 50$ L/g | OD1 | 1.36 | 0.46 | 66.2 |
| | OD2 | 1.36 | 0.54 | 60.3 |
| | OD3 | 1.05 | 0.55 | 47.6 |
| $K_D = 100$ L/g | OD1 | 1.36 | 0.49 | 63.9 |
| | OD2 | 1.36 | 0.60 | 55.9 |
| | OD3 | 1.05 | 0.58 | 44.8 |

$$RMSE = \sqrt{\frac{1}{N}\sum_{i=1}^{N}[\log_{10}(C_{sim}) - \log_{10}(C_{obs})]^2} \qquad (32)$$

[40] Here $C_{sim}$ and $C_{obs}$ are the simulated and observed EC concentrations, respectively.

[41] Comparisons between observations and model simulations are also presented in the form of probability plots in Figure 6 along with results for different values of the partition coefficient. As in Figure 5, the source uncertainty of $\pm 50\%$ is propagated to the beach sites and shown as error bands around the base case simulation (red solid line). EC partition coefficients of 1 and 10 L/g provided a good description of the observed data at all beach sites although all $K_D$ values describe the data better than the model that did not include sediment processes. The RMSE values for the different $K_D$ values and the two models are summarized in Table 4. Generally the lower value (1 L/g) described the low background values of EC better (Figures 6b and 6c) while the higher value (10 L/g) described the peaks better. Higher values of the partition coefficient (e.g., 50 or 100 L/g) represent conditions closer to raw wastewater [*Chapra*, 2008]. Burns Ditch in the Portage, Indiana area is known to receive more than 103 million gallons per day of discharge containing wastewater, contact and noncontact cooling water and stormwater from the US Steel and other facilities [*Portage Community News*, 2011]; therefore, it is not surprising that the higher values of partition coefficient such as 50 L/g provide a good description of the observed data. EC are also known to associate with a broad range of particle sizes and recent work seems to provide evidence [*Bucci et al*., 2011] for biphasic decay of EC with two populations—a recalcitrant EC population that resists decay and another population that undergoes decay readily. Since these complexities are not included in our models, it may be difficult to capture the behavior of EC over the entire range of values using a single $K_D$ value in the current formulation. To understand results in Figures 5 and 6 and to relate the peaks to the frequency of sediment resuspension events in our study area, we examined the bottom shear stress as a function of time. Figure 7 shows the net bottom shear stress (equation (25)) at N2, located slightly offshore of beach site OD2. The red dashed line denotes the critical

shear stress for erosion (0.1 N/m²) used in the numerical model. Several major resuspension events between JD 180 and JD 187 can be observed in the time series and the net critical shear stress for erosion was exceeded 23.1% of the total simulation time, however, the EC sampling frequency was inadequate to resolve the details of the EC peaks during these resuspension events (Figure 5). Analysis of wind direction (not shown) did not associate resuspension events with any particular wind direction. This is not surprising since bottom shear stress is dominated by waves.

[42] Since our model simulates fundamental particle processes and interactions between EC and sediment particles, the model can be used to understand how association with particles changes as a function of time and at different depths and distances from the shoreline. Concentrations of attached EC at two locations (nearshore and offshore) are shown in Figure 8. Results presented in the figure were obtained using a partition coefficient ($K_D$) of 10.0 L/g and the linear isotherm [*Bai and Lung*, 2005]. We notice that the water column is relatively uniform at the beach sampling sites closer to the shore (Figure 8b) where values of the attached fraction of bacteria are fairly similar in the top and bottom layers. This picture changes as we move away from the shore. As shown in Figure 8a, the bottom layers contain higher attached fraction of bacteria away from the shoreline. Closer examination revealed that although the mean concentration of SSC is higher nearshore compared to offshore locations, the bottom layers of the water column in the offshore region have higher SSC values due to cross-shore exchange of sediment and the slow deposition of finer particles away from the shore. As shown in equation (13), the attached fraction ($f_p$) is a function of the concentration of suspended sediment ($S$). As expected, the SSC concentration is more variable in the deeper waters (offshore). In shallower waters, the water column shows very little variation in the vertical. The mean value of $f_p$ in the offshore was 0.01 in the top layer and 0.09 in the bottom layer as shown in Figure 8. In the nearshore, the mean value of $f_p$ in the water column showed little variation and was 0.03 in the top layer and 0.04 in the bottom layer.

[43] Under favorable conditions, EC settling out of the water column can survive and continue to grow in the bottom sediment layer. The EC population in the sediment layer can then act as a secondary source of contamination. In the results presented here, growth rate in the sediment was set to zero. Despite a zero growth and inactivation rate, resuspension of EC in sediment significantly impacts EC concentrations in the water column. A direct comparison between the two models (with and without sediment-bacteria interactions) is shown using probability plots in Figure 6. The comparisons show that including sediment-bacteria interactions and explicitly modeling the SSC concentration and resuspension of bacteria (shown in Figure 5) significantly improves the model's ability to predict the median concentrations of EC. This is due to the fact that short-duration, low-intensity resuspension events are very common in our study area. The effect of these events is to raise the background values of EC producing multiple smaller EC peaks which cannot be captured by a model without sediment processes. The large EC peaks in our 1 month simulation period were captured by both models since those peaks were caused by elevated levels of EC
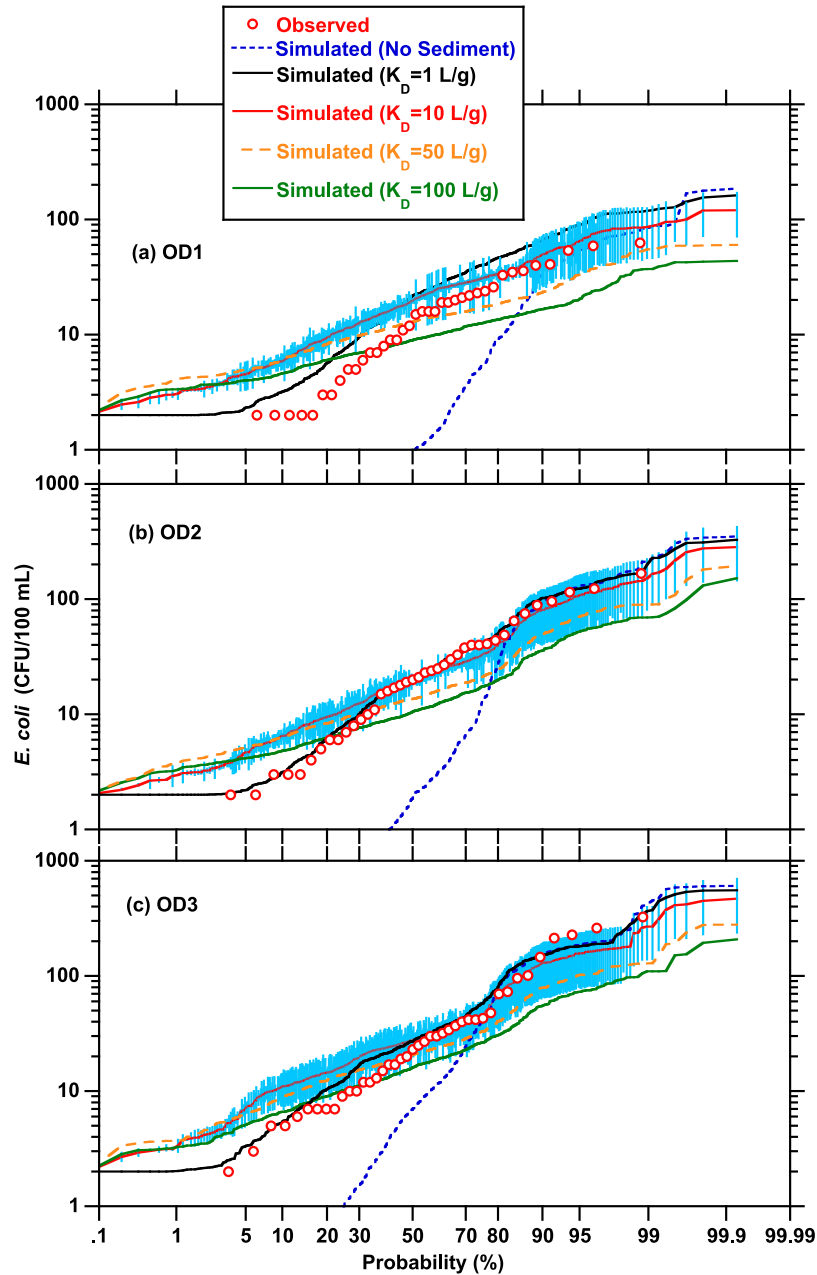
**Figure 6.** Probability plots for observed values of *Escherichia coli* (at OD1, OD2, and OD3) compared with results from simulations with and without sediment-bacteria interactions.
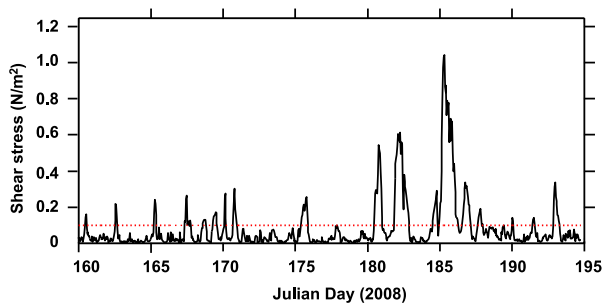


**Figure 7.** Bottom shear stress due to currents and waves at location N2. Dashed line denotes the critical shear stress for erosion above which resuspension events occur.

coming from the point-source at the Burns Ditch outfall. At least one large peak was probably caused by a large resuspension event (e.g., around JD 185) but the frequency of sampling was unable to resolve the details of the peaks during this major resuspension event.

[44] Finally, we discuss the limitations of the present study in order to identify areas for future refinement. While model performance significantly improved when we coupled the sediment and bacteria models, the model still did not predict several peaks. This is attributed to a number of factors described below: (a) the inability of the wave model to describe wave processes accurately within the breaking zone where EC samples are collected. Since the wave contribution to the net shear stress is significant, this is
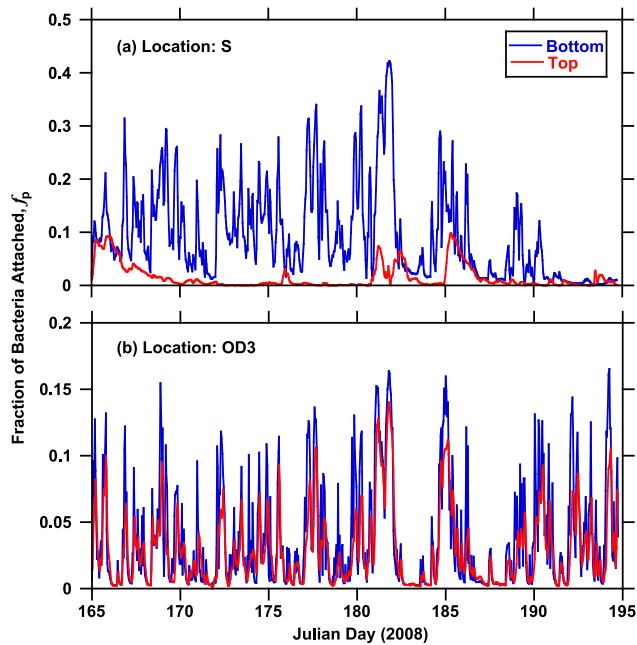
**Figure 8.** Attached fraction of *Escherichia coli* in the top and bottom layers at locations S (depth = 10 m) and N2 (depth = 5 m).

an important limitation of the current model, (b) we have not attempted a systematic parameter estimation of the fate and transport model due to computational demands of the fully three-dimensional model, therefore the set of parameters used to generate the results in Figures 5 and 6 are representative but not optimal, (c) uncertainties in model inputs including the settling velocity, sediment size classes with which bacteria are associated at our sites as well as the critical shear stress values used for erosion and deposition. Fractional filtration experiments combined with data from laser in situ scattering and transmissometry (LISST) instruments are expected to reduce the uncertainty, (d) some uncertainties are also associated with the ability of the tracer transport model in simulating transport accurately. In spite of these limitations, we were able to compare the performance of the two models since these uncertainties equally affect both models (with and without sediment processes).

## 4. Discussion

[45] Results from the three-dimensional circulation model, summarized in Table 1, show that nearshore hydrodynamics is accurately simulated by the three-dimensional nested-grid hydrodynamic model. Error (expressed as RMSE) in model-predicted values of alongshore and cross-shore velocities increases as the shoreline is approached, possibly due to the dominance of small-scale processes that are not adequately resolved by the turbulence models used as well as other processes such as wave-current interactions that are not explicitly represented in the model. More sophisticated turbulence closure models for the horizontal scales may improve performance of the transport model [*Thupaki et al.*, 2013].

[46] Southern Lake Michigan region is a low-wave energy environment compared to typical marine environ-

ments, and the average wave height was 0.2 m during the summer of 2008. However, due to the shallow bathymetry as well as occasional large waves, bottom shear stress due to waves accounts for the majority of the net bottom shear stress. A semiempirical parametric wave model was used to hindcast wind-generated surface waves and the resultant bottom shear stress. Figure 3 compares significant wave height predicted by the wave model with wave heights measured by ADCPs deployed in the offshore (M) and nearshore (S, N1, and N2) locations. While the model results compare well with observations, the comparisons show that the wave model generally under-predicts the peak wave height. In addition, as shown in Figures 3c and 3d, errors increase closer to the shoreline due to the absence of processes such as refraction and diffraction in the governing equations solved by the wave model. This is supported by values of RMSE for the model simulated wave height, presented in Table 1. Errors in interpolated wind fields can also result in large inaccuracies in wave models [*Komen et al.*, 1994]. In addition, our models do not include wave-current interactions or shallow water wave processes, which could be the source of some of the errors in the hydrodynamic model as well. Studies that focus on accurate modeling of wave-current interactions and nearshore processes would need to include a detailed description of these processes in the numerical wave model. The direction and power spectra of observed wave height (not shown in the paper) indicate that large waves generally approach from the north, which is also the direction of maximum fetch. This is consistent with the observations by *Lesht* [1989], who found that most sediment resuspension events in the Indiana Shoals occur during northerly winds.

[47] Values of suspended sediment concentration (SSC), presented in Figure 4, vary from about 2 mg/L to about 10 mg/L. The high SSC values seen around JD 182 and JD 185 correspond to the large wave-height measurements made by the nearshore ADCP (at location S). This suggests that high sediment content in the water column as far as 9 km from the shore could be caused by wave-induced resuspension events. This is consistent with past observations that associate large offshore sediment resuspension events in Lake Michigan with high wave activity associated with northerly winds [*Eadie et al.*, 2002; *Lesht*, 1989]. Comparison between model predictions and SSC values obtained from ADCP backscatter values presented in Figure 4 shows that the model is able to predict the mean suspended concentration reasonably well. Considering the measurement uncertainty in wave-height observations by the ADCP at the location S (RMSE = 0.1 m), these errors are within acceptable limits. The model is able to accurately describe the larger resuspension events around JD 182 and JD 185 which are associated with large (around 1 m) wave heights. Since wave-induced bottom shear stress dominates net bottom shear stress, using a more accurate wave model will improve SSC comparisons. Observations by *Lesht and Hawley* [1987] and *Lesht* [1989] suggest that the nearshore (<30 m) region is a low-depositional environment without significant sediment burial. Also, sensitivity analysis of a vertically integrated suspended sediment model by *Lee et al.* [2005] found that critical shear stresses for erosion and deposition, settling velocity, and sediment availability

strongly influenced suspended sediment concentration in Lake Michigan. As a result, accurately representing the resuspension process during low and medium wave activity is a challenging task. Model results might be improved by including a larger number of sediment size classes, sediment-flocculation, and nonlinear stress-resuspension relationships into the numerical model in addition to increasing the accuracy of the wave model.

[48] The Fourier norms presented in Table 3 show that the accuracy of the SSC model is correlated with the accuracy of wave model. We find that the SSC concentrations during the latter part of the simulation period (from about JD 180–200) are more accurately predicted by the model strongly suggesting that improving the wave model's accuracy is likely to improve the accuracy of the sediment transport (and by extension the bacteria fate and transport) model. It is also worth noting that the period (JD 160–180) is associated with a milder wave climate than the period (JD 180–200), which indicates that model performance is better during high wave heights.

[49] Sediment erodability values ($M$) of $10^{-5} - 5 \times 10^{-4}$ were noted for a sediment bed made of soft natural mud in the Severn Estuary [*Falconer and Chen*, 1996]; however, it is well known that the bed sediment composition (e.g., % sand, % mud) can change cohesiveness, therefore our value ($10^{-6}$ kg/m$^2$ s) appears to be reasonable for the depositional environment considered in this study. The critical shear stress values used in our work are within the range of values reported in the literature. There is evidence by *Stolzenbach et al.* [1992] to support the view that biological processes in the sediment layer make the bottom sediments more cohesive (i.e., less erodible). Using the same logic as was used in equation (2) (i.e., that rates of biological processes such as predation increase with temperature), it is possible to express the critical shear stresses ($\tau_{cr,\ ero}$ and $\tau_{cr,\ d}$) as functions of temperature; however, this approach was not used due to lack of site-specific data linking bed conditions to temperature.

[50] The conditions simulated in this study are representative of conditions present during the summer months, and a long-term simulation would be required to calculate reliable morphological trends in the bathymetry in southern Lake Michigan. The locations close to the shore reveal a more dynamic environment with large sediment fluxes (both deposition as well as erosion). This is consistent with the fact that bottom shear stresses due to waves decrease exponentially with depth. On average, the nearshore location is a low-depositional environment, while the deeper waters experience higher rates of sediment deposition.

[51] Errors in simulated concentrations of EC in knee-deep waters at the Ogden Dunes beaches (OD1, OD2, and OD3) using the two different bacterial fate and transport models (with and without sediment-bacteria interactions) are presented in Table 4. Error (measured as RMSE) of the model that simulates sediment-bacteria interactions is significantly lower and varies from 0.52 log$_{10}$(CFU/100 mL) at OD1 to 0.56 log$_{10}$(CFU/100 mL) at OD3, while RMSE of the model that does not include sediment transport varies from 1.36 log$_{10}$(CFU/100 mL) at OD1 to 1.05 log$_{10}$(CFU/ 100 mL) at OD3. The improvement in model accuracy at OD3 (closer to Burns Ditch) compared with OD1 (farther from Burns Ditch) suggests that closer to the outfall the

contaminant plume dynamics dominate all other secondary sources of contamination. This has also been observed in earlier studies [*Thupaki et al.*, 2013] that focus on simulating a conservative tracer (Rhodamine WT) in the nearshore region. Therefore, improvements in modeling the transport and mixing dynamics for a tracer are also likely to improve the results of the bacterial model.

[52] Simulated time series of EC concentrations at the Ogden Dunes beaches are compared with observed concentrations in Figure 5. The Burns Ditch outfall plume dynamics dominates the observed EC concentrations at the beaches. The comparison between the numerical models with and without sediment-bacteria interactions in Figure 5 indicate that including the sediment-bacteria interactions improves the overall accuracy of the bacterial fate and transport model by predicting the EC peaks due to small resuspension events. Several large sediment resuspension events were also observed around JD 180. However, water samples were not collected in inclement weather during this period and EC observations were therefore not adequate to resolve the details sufficiently.

[53] As mentioned earlier, sediment particles in the water column affect bacterial fate and transport directly as well as indirectly. Higher suspended sediment concentration increases settling rate of bacteria attached to sediment particles and at the same time reduces inactivation of bacteria due to solar radiation. The results presented in Figures 5 and 6 show that the overall impact of explicitly simulating sediment-bacteria interactions, in the absence of a significant resuspension event, is a lower peak EC level. However, this observation depends on the relative importance of sediment as a source of EC at any particular site. Figure 8 shows the dynamic nature of the attached fraction as a function of space and time, therefore assuming a constant and time-invariant attached fraction misrepresents the settling losses.

[54] Comparisons between the two models (with and without sediment) and EC observations are shown in Figure 6 as probability plots. Compared to the time series plots (Figure 5) which show the same comparison, the probability plots bring out the importance of including sediment-bacteria interactions in the modeling as the model with sediment processes follows the same trend as the observations. Higher median values of EC concentration in results from the model with sediment-bacteria interactions are a result of the models ability to simulate small-scale peaks due to resuspension better (Figure 5). At the same time, the peak values predicted by the model with sediment-bacteria interactions are generally lower due to higher settling losses. Therefore, the model with sediment-bacteria interactions constrains the EC fate and transport processes by preventing EC levels from reaching unreasonably high values. We are able to make this observation as the loss processes due to base mortality and light-based inactivation in both models used the same set of rates obtained from our field experiments.

[55] The sediment layer is usually nutrient rich and provides a more hospitable environment for EC than the water column and this could result in regrowth of bacteria in the sediment. *Craig et al.* [2004] have examined the persistence and growth of EC in coastal sediment and their influence on recreational water quality and found that EC may persist for more than 28 days in coastal sediments. For the simulations presented here, initial bacteria content in the

bottom sediment layer was calculated by running the model through a spin-up period and assuming zero net growth and inactivation in the sediment. We found that the model performance was very sensitive to the initial concentration of EC per unit mass of sediment (CFU/kg). However, this value soon reached a dynamic equilibrium with EC concentration entering from the outfall and resuspension due to waves and currents. More accurate representations of growth/inactivation rates of bacteria in the sediment layer (as well as long-term input conditions at sources) would be necessary in order to estimate the rate of removal of bacteria from the bottom sediment layer.

[56] Removal of EC from the water column due to settling is a major factor in the total loss rate of EC in the water column [*Thupaki et al.*, 2010]. Modeling attached EC (the fraction that settles into the bottom sediment layer) is, therefore, important. The magnitude of attached EC is highly variable. Figure 8 shows the fraction of attached EC at two locations (nearshore and offshore). At offshore locations, the attached fraction displays a much higher variability in the vertical. Mean value at location S was 0.09 in the bottom layer and 0.01 in the surface layer. In the nearshore, the variation in the vertical was negligible with an $f_p$ value of 0.03 in the top layer and 0.04 in the bottom layer. As described by a linear isotherm (equation (12)), the attached fraction depends mainly on the suspended sediment concentration. The top layers with lower SSC concentration presented fewer attachment sites for bacteria and therefore have a lower attached fraction. Higher concentrations of the attached fraction increase the rate of EC removal from the water column due to settling. In general, this implies that EC losses due to settling are lower in the relatively clear offshore (surface) waters than in the nearshore region; however, due to offshore transport of suspended sediment and accumulation of suspended sediment in the bottom layers, the attached fraction of EC in the bottom layers of the offshore waters can be very high. Therefore, coupled suspended sediment-bacteria modeling is extremely important to describing EC fate and transport in the water column as is an accurate description of the attached and unattached fractions of bacteria in the water column.

## 5. Conclusion

[57] We used a bacterial fate and transport model coupled with a sediment transport model to assess the role of sediment-bacteria interactions on EC concentration at several beaches in southern Lake Michigan where samples were collected from knee-deep waters. We found that EC from the nearshore Burns Ditch outfall was the principal source of EC contamination at the beaches. Plume dynamics dominated the EC concentrations close to the outfall. Farther from the outfall the accuracy of the transport model was lower for both models (i.e., with and without sediment interactions) this is probably related to the model's ability to describe a conservative tracer as described in the work of *Thupaki et al.* [2010]. Including sediment-bacteria interactions in the bacterial fate and transport model improved the accuracy of the numerical model as quantified by the RMSE. ADCP observations show that the mean wave height in southern Lake Michigan was about 0.21 m in the nearshore region. However, despite being characterized as a low-wave energy environment, shear stress for erosion exceeded

the critical value 23% of the total simulation period, hence resuspension of EC from the bottom sediment was an important process. The GLERL-Donelan wave model underpredicts the wave heights and consequently the bottom shear stresses [*Hawley et al.*, 2004]. Improving the accuracy of the wave model can be expected to further improve the simulations. Mean background concentrations were simulated better by including interactions between sediment and bacteria. Dynamically calculating the concentrations of attached EC using results from the SSC model described the variability of the attached fraction within the water column better. Results show that resuspension can explain observed EC concentrations better than just the outfall dynamics, especially at sites far from the outfall. Resuspension represents an important secondary source of EC contamination, depending on the bacterial survival and regrowth rates in the sediment. Using the linear isotherm model for EC attachment-detachment dynamics, we found that the fraction of attached EC that experiences temporary removal from the water column due to settling is highly variable in the vertical as well as between the offshore and nearshore regions. Our results indicate that including sediment-bacteria interactions significantly improves the overall ability of the model to predict EC concentrations at beach sites.

## Appendix A: Details of the Wave Model

[58] Wave climate was simulated using a semiparametric wave model described in the work of *Donelan* [1977] and *Schwab et al.* [1984]. Equation (A1) solves the wave momentum transport equations in the horizontal $(x, y)$ directions and includes momentum input into the water column by wind shear at the surface:

$$\frac{\partial M_x}{\partial t} + c_x \frac{\partial M_x}{\partial x} + c_y \frac{\partial M_x}{\partial y} = \frac{\tau_x}{\rho_w}$$
$$\frac{\partial M_y}{\partial t} + c_x \frac{\partial M_y}{\partial x} + c_y \frac{\partial M_y}{\partial y} = \frac{\tau_y}{\rho_w} \tag{A1}$$

where $\rho_w$ is the density of water and $(M_x, M_y)$ are wave momentum components of the momentum vector $\boldsymbol{M}$, $(c_x, c_y)$ are the group velocity components, and $(\tau_x, \tau_y)$ are the wind shear stress components in $(x, y)$ directions. The wave momentum components are calculated from the net energy of the wave field $E(f, \theta)$ using equation (A2).

$$M_x = g \int_0^\infty \int_0^{2\pi} \frac{E(f, \theta)}{c(f)} \cos\theta \, d\theta \, df$$
$$M_y = g \int_0^\infty \int_0^{2\pi} \frac{E(f, \theta)}{c(f)} \sin\theta \, d\theta \, df \tag{A2}$$

where $\theta$ is the wave direction, $f$ is the frequency, and $c(f)$ is the phase speed of the wave component. Using the linear wave theory for deep water waves, the wave momentum flux can be calculated using equation (A3)

$$c_x M_x = \frac{|\boldsymbol{M}| c_p}{4} \cos^2\theta_0 + \frac{1}{2} \tag{A3}$$

$$c_x M_y = c_y M_x = \frac{|\boldsymbol{M}| c_p}{4} \cos\theta_0 \sin\theta_0$$

$$c_y M_y = \frac{|\boldsymbol{M}|c_p}{4}\sin^2\theta_0 + \frac{1}{2}$$

[59] Here $c_p$ is the phase velocity of the peak frequency and $\theta_0$ is the angle between wind vector and wave direction. To solve equation (A1), a relation between wave momentum and wave height is needed. An empirical relation derived from JONSWAP relations is used [*Komen et al.*, 1994]. Momentum input from wind $(\tau_x, \tau_y)$ is determined based on wind speed and waveform [*Donelan*, 1977]. The wave model solves the equations on a uniform Cartesian grid using explicit forward time stepping and a combination of upwind and centered difference methods to discretize advection terms [*Schwab et al.*, 1984]. The wave model has been shown to predict accurately wave characteristics for fetch-limited conditions in low-wave energy environments such as Lake Michigan. More details of the model implementation and performance are available in the works of *Schwab et al.* [1984] and *Liu et al.* [1984, 2002].

## Notation

### Wave Model

| | |
|---|---|
| $(M_x, M_y)$ | wave momentum components. |
| $(c_x, c_y)$ | wave group velocity components. |
| $(\tau_x, \tau_y)$ | wind shear stress components. |
| $E(f, \theta)$ | wave energy spectrum. |
| $\theta$ | wave direction. |
| $f$ | wave frequency. |
| $C(f)$ | phase velocity of wave component. |

### Sediment-Bacteria Interactions Model

| | |
|---|---|
| $C_T$ | net EC concentration in water column, CFU/m$^3$. |
| $C_D$ | concentration of unattached EC, CFU/m$^3$. |
| $C_P$ | concentration of attached EC, CFU/m$^3$. |
| $\zeta$ | mass-specific concentration of attached EC, CFU/kg. |
| $K_D$ | partition coefficient for EC, L/g. |
| $f_P$ | fraction of attached EC, nondimensional. |
| $f_D$ | fraction of unattached EC, nondimensional. |
| $F_{SC}$ | settling flux for EC, CFU/m$^2$ s. |
| $F_{RC}$ | resuspension flux for EC, CFU/m$^2$ s. |
| $C_{sed}$ | concentration of EC in the bottom sediment layer |
| $S$ | suspended sediment concentration in water column, kg/m$^3$. |
| $F_{SS}$ | settling flux for suspended sediment in the water column, kg/m$^2$ s. |
| $F_{RS}$ | resuspension flux for suspended sediment in the water column, kg/m$^2$ s. |
| $m_{sed}$ | mass of sediment in the bottom sediment layer, kg/m$^2$. |

### Bacteria Inactivation Model

| | |
|---|---|
| $k_{net}$ | net inactivation rate for EC, s$^{-1}$. |
| $K_I$ | inactivation of EC due to solar radiation, s$^{-1}$. |
| $I_0$ | solar radiation, W/m$^2$ s. |
| $k_e$ | light extinction coefficient in the water column, m$^{-1}$. |
| $k_d$ | base mortality for EC in the water column, s$^{-1}$. |
| $\theta_M$ | mortality temperature multiplier. |

## References

Abu-Ashour, J. S. (1994), Movement of bacteria in agricultural wastewater through the soil matrix and macropores, PhD thesis, pp. 219, Univ. of Guelph, Canada.

American Public Health Association (APHA) (1998), *Standard Methods for the Examination of Water and Wastewater*, 20th ed., Am. Public Health Assoc., Washington, D. C.

Auer, M. T., and S. L. Niehaus (1993), Modeling fecal coliform bacteria. 1: Field and laboratory determination of loss kinetics, *Water Res.*, *27*, 693–701.

Bai, S., and W. S. Lung (2005), Modeling sediment impact on the transport of fecal bacteria, *Water Res.*, *39*(20), 5232–5240.

Blumberg, A. F., and G. L. Mellor (1987), A description of a three-dimensional coastal ocean circulation model, in *Three-Dimensional Coastal Ocean Models*, edited by N. S. Heaps, pp. 1–16, AGU, Washington, D. C.

Brown, J. S., E. D. Stein, D. Ackerman, J. H. Dorsey, J. Kyon, and P. M. Carter (2013), Metals and bacteria partitioning to various size particles in Ballona creek storm water runoff, *Environ. Toxicol. Chem.*, *32*(2), 320–328, doi:10.1002/etc.2065.

Bucci, V., M. Vulić, X. Ruan, and F. L. Hellweger (2011), Population dynamics of *Escherichia coli* in surface water, *J. Am. Water Res. Assoc.*, *47*, 611–619, doi:10.1111/j.1752-1688.2011.00528.x.

Burban, P.-Y., Y.-J. Xu, J. McNeil, and W. Lick (1990), Settling speeds of flocs in fresh water and seawater, *J. Geophys. Res.*, *95*, 18,213–18,220.

Chao, X., Y. Jia, F. D. Shields Jr., S. S. Y. Wang, and C. M. Cooper (2008), Three-dimensional numerical modeling of cohesive sediment transport and wind wave impact in a shallow oxbow lake, *Adv. Water Res.*, *31*(7), 1004–1014.

Chapra, S. C. (2008), *Surface Water-Quality Modeling*, Waveland Press, Long Grove, IL.

Characklis, G. W., M. J. Dilts, O. D. Simmons, C. A. Likirdopulos, L. A. H. Krometis, and M. D. Sobsey (2005), Microbial partitioning to settleable particles in stormwater, *Water Res.*, *39*(9), 1773–1782.

Craig, D. L., H. J. Fallowfield, N.J. Cromar (2004), Use of microcosms to determine persistence of Escherichia coil in recreational coastal water and sediment and validation with in situ measurements, *J. Appl. Microbiol.*, *96*(5), 922–930, doi: 10.1111/j.1365-2672.2004.02243.x.

Davies, C. M., J. A. H. Long, M. Donald, and N. J. Ashbolt (1995), Survival of fecal microorganisms in marine and fresh-water sediments, *Appl. Environ. Microbiol.*, *61*(5), 1888–1896.

de Brauwere, A., B. de Brye, P. Servais, J. Passerat, and E. Deleersnijder (2011), Modelling *Escherichia coli* concentrations in the tidal Scheldt river and estuary, *Water Res.*, *45*(9), 2724–2738.

Decho, A. W. (2000), Microbial biofilms in intertidal systems: An overview, *Cont. Shelf Res.*, *20*, 1257–1273.

Desmarais, T. R., H. M. Solo-Gabriele, and C. J. Palmer (2002), Influence of soil on fecal indicator organisms in a tidally influenced subtropical environment, *Appl. Environ. Microbiol.*, *68*(3), 1165–1172.

Donelan, M. A. (1977), *A Simple Numerical Model for Wave and Wind Stress Prediction*, 28 pp., Natl. Water Res. Inst., Ont.

Droppo, I. G., S. N. Liss, D. Williams, T. Nelson, C. Jaskot, and B. Trapp (2009), Dynamic existence of waterborne pathogens within river sediment compartments: Implications for water quality regulatory affairs, *Environ. Sci. Technol.*, *43*(6), 1737–1743.

Eadie, B. J. (1997), Probing particle processes in Lake Michigan using sediment traps, *Water Air Soil Pollut.*, *99*, 133–139.

Eadie, B. J., et al. (2002), Particle transport, nutrient cycling, and algal community structure associated with a major winter-spring sediment resuspension event in southern Lake Michigan, *J. Great Lakes Res.*, *28*, 324–337.

Falconer, R. A., and Y. Chen (1996), Modeling sediment transport and water quality processes on todal flood plains, in *Floodplain Processes*,

edited by M. G. Anderson, D. E. Walling, and P. D. Bates, chap. 14, pp. 361–398, John Wiley & Sons, Chichester, pp. 361–398.

Feng, Z., A. Reniers, B. K. Haus, and H. M. Solo-Gabriele (2013), Modeling sediment-related enterococci loading, transport and inactivation at an embayed, non-point source beach, *Water Resour. Res.*, *49*, 1–20, doi: 10.1029/2012WR012432.

Fujioka, R., C. Sian-Denton, M. Borja, J. Castro, and K. Morphew (1998), Soil: The environmental source of *Escherichia coli* and enterococci in Guam's streams, *J. Appl. Microbiol.*, *85*(S1), 83S–89S.

Gantzer, C., L. Gillerman, M. Kuznetsov, and G. Oron (2001), Adsorption and survival of faecal coliforms, somatic coliphages and F-specific RNA phages in soil irrigated with wastewater, *Water Sci. Technol.*, *43*(12), 117–124.

Gao, G., R. A. Falconer, and B. Lin (2011), Numerical modelling of sediment-bacteria interaction processes in surface waters, *Water Res.*, *45*(5), 1951–1960.

Gao, G., R. A. Falconer, and B. Lin (2013), Modelling importance of sediment effects on fate and transport of enterococci in the Severn Estuary, UK, *Mar. Pollut. Bull.*, *67*(1–2), 45–54, doi:10.1016/j.marpolbul.2012.12.002.

Ge, Z., M. B. Nevers, D. J. Schwab, and R. L. Whitman (2010), Coastal loading and transport of *Escherichia coli* at an embayed beach in Lake Michigan, *Environ. Sci. Technol.*, *44*(17), 6731–6737.

Ge, Z., R. L. Whitman, M. B. Nevers, and M. S. Phanikumar (2012a), Wave-induced mass transport affects daily *Escherichia coli* fluctuations in nearshore water, *Environ. Sci. Technol.*, *46*(4), 2204–2211.

Ge, Z., R. L. Whitman, M. B. Nevers, M. S. Phanikumar, and M. N. Byappanahalli (2012b), Nearshore hydrodynamics as loading and forcing factors for *Escherichia coli* contamination at an embayed beach, *Limnol. Oceanogr.*, *57*(1), 362–381.

Ginn, T. R., B. D. Wood, K. E. Nelson, T. D. Scheibe, E. M. Murphy, and T. P. Clement (2002), Processes in microbial transport in the natural subsurface, *Adv. Water Resour.*, *25*(8–12), 1017–1042.

Guber, A. K., D. R. Shelton, and Y. A. Pachepsky (2005), Effect of manure on *Escherichia coli* attachment to soil, *J. Environ. Qual.*, *34*, 2086–2090.

Hardina, C. M., and R. S. Fujioka (1991), Soil: The environmental source of *Escherichia coli* and enterococci in Hawaii's streams, *Environ. Toxicol. Water Qual.*, *6*(2), 185–195.

Hawley, N., B. M. Lesht, and D. J. Schwab (2004), A comparison of observed and modeled surface waves in southern Lake Michigan and the implications for models of sediment resuspension, *J. Geophys. Res.*, *109*, C10S03, doi:10.1029/2002JC001592.

Hipsey, M. R., J. D. Brookes, R. H. Regel, J. P. Antenucci, and M. D. Burch (2006), In situ evidence for the association of total coliforms and *Escherichia coli* with suspended inorganic particles in an Australian reservoir, *Water Air Soil Pollut.*, *170*, 191–209.

Jamieson, R., D. M. Joy, H. Lee, R. Kostaschuk, and R. Gordon (2005), Transport and deposition of sediment associated *Escherichia coli* in natural streams, *Water Res.*, *39*, 2665–2675, doi:10.1016/j.watres.2005.04.040.

Jeng, H. C., A. J. England, and H. B. Bradford (2005), Indicator organisms associated with stormwater suspended particles and estuarine sediment, *J. Environ. Sci. Health*, *40*, 779–791, doi:10.1081/ESE-200048264.

King, B. J., D. Hoefel, D. P. Damináto, S. Fanok, and P. T. Monis (2008), Solar UV reduces Cryptosporidium parvum oocyst infectivity in environmental waters, *J. Appl. Microbiol.*, *104*, 1311–1323.

Kirchman, D. (1983), The production of bacteria attached to particles suspended in a freshwater pond, *Limnol. Oceanogr.*, *28*(5), 858–872.

Komen, G. J., L. Cavaleri, M. Donelan, K. Hasselmann, S. Hasselmann, and P. Janssen (1994), *Dynamics and Modelling of Ocean Waves*, p. 512, Cambridge Univ. Press, Cambridge, U. K.

Krometis, L. H., G. W. Characklis, O. D. Simmons, M. J. Dilts, C. A. Likirdopulos, and M. D. Sobsey (2007), Intra-storm variability in microbial partitioning and microbial loading rates, *Water Res.*, *41*, 506–516.

Krone, R. B. (1962), Flume studies of the transport of sediment in estuarial shoaling processes, Final Report, Hydraul. Eng. Lab., Univ. of Calif., Berkeley.

LaBelle, R. L., C. P. Gerba, S. M. Goyal, J. L. Melnick, I. Cech, and G. F. Bogdan (1980), Relationships between environmental factors, bacterial indicators, and the occurrence of enteric viruses in estuarine sediments, *Appl. Environ. Microbiol.*, *39*(3), 588–596.

Lee, C., D. J. Schwab, and N. Hawley (2005), Sensitivity analysis of sediment resuspension parameters in coastal area of southern Lake Michigan, *J. Geophys. Res.*, *110*, C03004, doi:10.1029/2004JC002326.

Lee, C., D. J. Schwab, D. Beletsky, J. Stroud, and B. Lesht (2007), Numerical modeling of mixed sediment resuspension, transport, and deposition during the March 1998 episodic events in southern Lake Michigan, *J. Geophys. Res.*, *112*, C02018, doi:10.1029/2005JC003419.

Lesht, B. M. (1989), Climatology of sediment transport on Indiana Shoals, Lake Michigan, *J. Great Lakes Res.*, *13*, 486–497.

Lesht, B. M., and N. Hawley (1987), Near-bottom currents and suspended sediment concentration in southern Lake Michigan, *J. Great Lake Res.*, *13*, 375–386.

Li, J., and L. McLandsborough (1999), The effects of the surface charge and hydrophobicity of *Escherichia coli* on its adhesion to beef muscle, *Int. J. Food Microbiol.*, *53*(2–3), 185–193.

Lindqvist, R., and C. G. Enfield (1992), Cell-density and nonequilibrium sorption effects on bacterial dispersal in groundwater microcosms, *Microb. Ecol.*, *24*(1), 25–41.

Liu, P. C., D. J. Schwab, and J. R. Bennett (1984), Comparison of a two-dimensional wave prediction model with synoptic measurements in Lake Michigan, *J. Physical Oceanography*, *14*, 1514–1518.

Liu, P. C., D. J. Schwab, and R. E. Jensen (2002), Has wind-wave modeling reached its limit?, *Ocean Eng.*, *29*(1), 81–98.

Liu, L., M. S. Phanikumar, S. L. Molloy, R. L. Whitman, M. B. Nevers, D. A. Shively, D. J. Schwab, and J. B. Rose (2006), Modeling the transport and inactivation of *E. coli* and enterococci in the nearshore region of Lake Michigan, *Environ. Sci. Technol.*, *40*(16), 5022–5028, doi:10.1021/es060438k.

Luettich, R. A., D. R. F. Harleman, and L. Somlyody (1990), Dynamic behavior of suspended sediment concentrations in a shallow lake perturbed by episodic wind events, *Limnol. Oceanogr.*, *35*(5), 1050–1067.

Lumborg, U. (2005), Modelling the deposition, erosion, and flux of cohesive sediment through Øresund, *J. Mar. Syst.*, *56*, 179–193.

Lytle, D. A., E. W. Rice, C. H. Johnson, and K. R. Fox (1999), Electrophoretic mobilities of *Escherichia coli* O157: H7 and wild-type *Escherichia coli* strains, *Appl. Environ. Microbiol.*, *65*(7), 3222–3225.

Mehta, A. J. (1993), Hydraulic behaviour of fne sediment, *in Coastal, Estuarial and Harbour Engineers' Reference Book*, edited by M. B. Abbott and W. A. Price, pp. 577–584, E. & F.N. Spon Ltd., London.

Mehta, A. J., and E. Partheniades (1975), An investigation of the depositional properties of flocculated fine sediment, *J. Hydraul. Res.*, *13*(4), 361–381.

Mellor, G. L., and T. Yamada (1982), Development of a turbulence closure model for geophysical fluid problems, *Rev. Geophys.*, *20*, 851–875.

Phillips, M. C., H. M. Solo-Gabriele, A. M. Piggot, J. S. Klaus, and Y. Zhang (2011), Relationships between sand and water quality at recreational beaches, *Water Res.*, *45*(20), 6763–6769.

Portage Community News Item (2013), *Wastewater Permit is Issued for U.S. Steel Midwest Plant*. The Times Media Company, Porter, Indiana. [Available at http://www.nwitimes.com/news/local/porter/portage/wastewater-permit-is-issued-for-u-s-steel-midwest-plant/article_5652ce2d-ccc4–58ac-bac8-d4926bdb9e52.html, last accessed 20 September 2013.]

Reddy, H. L., and R. M. Ford (1996), Analysis of biodegradation and bacterial transport: Comparison of models with kinetic and equilibrium bacterial adsorption, *J. Contam. Hydrol.*, *22*(3–4), 271–287.

Rehmann, C. R., and M. L. Soupir (2009), Importance of interactions between the water column and the sediment for microbial concentrations in streams, *Water Res.*, *43*, 4579–4589, doi:10.1016/j.watres.2009.06.049.

Rijn, L. C. van (1989), Handbook sediment transport by currents and waves, Report, Delft Hydraul.

Roper, M. M., and K. Marshall (1979), Effects of salinity on sedimentation and of participates on survival of bacteria in estuarine habitats, *Geomicrobiol. J.*, *1*(2), 103–116.

Sanders, B. F., F. Arega, and M. Sutula (2005), Modeling the dry-weather tidal cycling of fecal indicator bacteria in surface waters of an intertidal wetland, *Water Res.*, *39*(14), 3394–3408.

Savage, W. G. (1905), Bacteriological examination of tidal mud as an index of pollution of the river, *J. Hygiene*, *5*(2), 146–174.

Scholl, M.A., R.W. Harvey, Laboratory investigations on the role of sediment surface and groundwater chemistry in transport of bacteria through a contaminated sandy aquifer, *Env, Sci. & Technol.*, *26*(7), 1410–1427, doi:10.1021/es00031a020.

Schwab, D. J., J. R. Bennett, P. C. Liu, and M. A. Donelan (1984), Application of a simple numerical wave prediction model to Lake Erie, *J. Geophys. Res.*, *89*, 3586–3592.

Sherer, B. M., R. Miner, J. A. Moore, and J. C. Buckhouse (1992), Indicator bacterial survival in stream sediments, *J. Environ. Qual.*, *21*, 591–595.

Sinton, L. W. (2005), Biotic and abiotic effects, in *Oceans and Health: Pathogens in the Marine Environment*, edited by S. Belkin and R. R. Colwell, pp. 69–92, Springer, New York.

Sinton, L. W., C. H. Hall, P. A. Lynch, and R. J. Davies-Colley (2002), Sunlight inactivation of fecal indicator bacteria and bacteriophages from waste stabilization pond effluent in fresh and saline waters, *Appl. Environ. Microbiol.*, *68*, 1122–1131.

Smagorinsky, J. (1963), General circulation experiments with the primitive equations. 1: The basic experiment, *Mon. Weather Rev.*, *91*(3), 99–164.

Soupir, M. L., S. Mostaghimi, and N. G. Love (2008), Method to partition between attached and unattached *E. coli* in runoff from agricultural lands, *J. Am. Water Resour. Assoc.*, *44*(6), 1591–1599.

Stolzenbach, K. D., K. A. Newman, and C. S. Wong (1992), Aggregation of fine particles at the sediment-water interface, *J. Geophys. Res.*, *97*, 17,889–17,898.

Thupaki, P., M. S. Phanikumar, D. Beletsky, D. J. Schwab, M. B. Nevers, and R. L. Whitman (2010), Budget analysis of *Escherichia coli* at a Southern Lake Michigan Beach, *Environ. Sci. Technol.*, *44*(3), 1010–1016.

Thupaki, P., M. S. Phanikumar, and R. L. Whitman (2013), Solute dispersion in the coastal boundary layer of Southern Lake Michigan, *J. Geophys. Res.*, *118*, 1606–1617, doi:10.1002/jgrc.20136.

Vallis, G. K. (2006), *Atmospheric and Oceanic Fluid Dynamics*, 745 pp., Cambridge Univ. Press, Cambridge, U. K.

Wall, G. R., Nystrom, E. A., and L. Simon (2006), Use of an ADCP to compute suspended-sediment discharge in the tidal Hudson River, New York, *U. S. Geol. Surv. Sci. Invest. Rep., 2006-5055*, 16 pp.

Whitman, R. L., and M. B. Nevers (2003), Foreshore sand as a source of *Escherichia coli* in nearshore water of a Lake Michigan beach, *Appl. Environ. Microbiol.*, *69*(9), 5555–5562.

Wu, Y., R. A. Falconer, and B. Lin (2005), Modelling trace metal concentration distributions in estuarine waters, *Estuarine Coastal Shelf Sci.*, *64*(4), 699–709.